Characterisation of Subfractions of Asphaltenes Extracted from an Oil Sand using NMR, DEPT and MALDI-TOF

Ce Zheng[1], Mingming Zhu[1]*, Reza Zareie[2] and Dongke Zhang[1]

[1] Centre for Energy (M473) and [2] School of Chemistry and Biochemistry (M313), The University of Western Australia, 35 Stirling Highway, Crawley, WA 6009, Australia

(A manuscript offered to ***Journal of Petroleum Science and Engineering***)

* Corresponding author:
Dr Mingming Zhu
Email: mingming.zhu@uwa.edu.au
Phone: +61 8 6488 5528
Fax: +61 8 6488 7622

Abstract

This paper reports the findings of an investigation into molecular structures and properties of an oil sand asphaltene sample and its subfractions. The asphaltene sample extracted from Buton Oil Sand (Indonesia) was fractionated stepwise into four subfractions by precipitation in a binary solvent system made from mixtures of dichloromethane/*n*-heptane with volumetric ratios of 30/70, 20/80 and 10/90, respectively. The average molecular structural parameters, including the average polycyclic aromatic hydrocarbon size, average side chain length and average molecular weight of the oil sand asphaltene sample and its subfractions, were measured and compared, using characterisation data obtained from nuclear magnetic resonance in combination with distortionless enhancement by polarisation transfer. The molecular weight distributions of the asphaltene samples were measured using a matrix-assisted laser desorption/ionisation time-of-flight mass spectrometry. The results indicated that the island molecular architecture was featured in all the asphaltene samples. The average polycyclic aromatic hydrocarbon size was found to be 7 rings for the least soluble subfraction, 6 rings for the other subfractions and the oil sand asphaltenes. The fractionation mechanism was dictated by polarity difference amongst subfractions as a result of relative luxuriance of the aliphatic parts. The use of ^{13}C NMR, DEPT and MALDI-TOF was shown to provide a useful means for characterisation and estimation of molecular structures of the asphaltenes.

Keywords: Asphaltenes; DEPT; Molecular structure; NMR; Oil sand; Fractions

1. Introduction

In dealing with heavy petroleum resources, asphaltenes are the most refractory compounds among all the petroleum fractions that often lead to many operational challenges from extraction to refining, exemplified by reservoir damage, well plugging, pipeline blockage, sediment formation in tanks and tankers and, during refining and processing, catalyst deactivation, reactor failure and plant outage (Ancheyta et al., 2010; Mullins, 2007). Although there has been a remarkable progress in the continuing effort to understand the fundamental properties of asphaltenes (Mullins, 2010, 2011; Mullins et al., 2012), the level of knowledge about the molecular structures of asphaltenes is still in a nascent stage. In the meantime, oil sand, also known as tar sand or bituminous sand, is an unconventional resource of liquid hydrocarbons that has received less attention. The bitumen extracted from oil sand is very viscous and sticky because of its high content of asphaltenes. While extensive studies have been carried out on petroleum asphaltenes and coal-derived asphaltenes (Andrews et al., 2011; Artok et al., 1999; Begon et al., 2003; Christopher et al., 1996; Clutter et al., 1972; Dickinson, 1980; Fergoug and Bouhadda, 2014; Kaminski et al., 2000; Masuda et al., 1996; Michon et al., 1997; Sanchez-Minero et al., 2013; Sheremata et al., 2004; Snape et al., 1979; Tojima et al., 1998; Trejo et al., 2007; Trejo et al., 2004), more effort has been called for in order to understand the chemical structures of asphaltenes in oil sand.

As a complex mixture, the polydispersity of asphaltenes has greatly hampered the progress of its characterisation studies. A great deal of work has been conducted on fractionation of asphaltenes in the past (Andersen et al., 1997; Andreatta et al., 2005; Buch et al., 2003; Buenrostro-Gonzalez et al., 2002; Dickie and Yen, 1967; Groenzin et al., 2003; Jacobs and Filby, 1983; Kaminski et al., 2000; Nalwaya et al., 1999; Ovalles et al., 2012; Petrova et al., 2013; Tojima et al., 1998; Trejo et al., 2004; Wiehe and Liang, 1996; Yang and Eser, 1999). In the literature, binary solvent systems are commonly used to fractionate asphaltenes. Tojima et al. (1998) used a toluene/heptane system to fractionate asphaltenes into heavy and light subfractions. In their findings, the least soluble subfraction defined as heavy asphaltenes, consisted of the most highly condensed polycyclic

aromatic hydrocarbons (PAHs) in the asphaltenes. Trejo et al. (2004) used the same binary solvent system to fractionate asphaltenes and compared the elemental composition across different fractions. Kaminski et al. (2000) reported fractionation work using a dichloromethane (DCM)/*n*-pentane system, in which the asphaltenes were firstly dissolved in DCM and then precipitated stepwise by adding increasing amounts of *n*-pentane. The precipitates were collected as subfractions by filtration when the DCM-to-*n*-pentane volumetric ratio reaching 30/70, 25/75, 20/80 and 10/90, respectively. Their results showed that the most polar subfraction (30/70) was not as soluble as the least polar subfraction (10/90). In addition, they also reported that unfractionated asphaltene samples appear to behave as a sum of their subfractions.

Many previous reports have discussed the trends amongst subfractions when using similar binary solvent systems, for example aromaticity was found to monotonically increase across subfractions with decreasing solubility and H/C ratio (Buch et al., 2003; Buenrostro-Gonzalez et al., 2002; Jacobs and Filby, 1983; Kaminski et al., 2000; Ovalles et al., 2012; Petrova et al., 2013; Tojima et al., 1998; Trejo et al., 2004; Yang and Eser, 1999). However effort to compare the subfractions in terms of their structural differences and use this approach to further probe the fractionation/precipitation mechanisms are scarce.

Among the spectroscopic techniques applied in characterising complex compounds, nuclear magnetic resonance (NMR) has been shown to have the potential for revealing the chemical nature of asphaltenes. Clutter and co-workers (1972) developed a technical method and protocol to characterise petroleum fractions with ^{1}H and ^{13}C NMR. They examined "aromaticity" through measuring aromatic carbon as a fraction of the total carbon, and brought forward a series of structural parameters, such as average number of aromatic rings and average number of alkyl substituents of an "average molecule". Snape and Ladner (1979) compiled a survey of ^{13}C chemical shift in aromatic hydrocarbons in coal-derived materials. Since then a large body of literature on asphaltene molecular parameters using ^{13}C NMR has been reported (Artok et al., 1999; Begon et al., 2003; Buenrostro-Gonzalez et al., 2001; Calemma et al., 1995; Christopher et al., 1996; Dickinson,

1980; Fergoug and Bouhadda, 2014; Gillet et al., 1980; Korb et al., 2013; Masuda et al., 1996; Michon et al., 1997; Myhr et al., 1990; Netzel, 1987; Ostlund et al., 2004; Rafenomanantsoa et al., 1994; Sanchez-Minero et al., 2013; Sheremata et al., 2004; Storm et al., 1994; Trejo et al., 2007; Yoshida et al., 1980). Likewise, since its introduction in 1988, laser desorption ionisation mass spectrometry has been increasingly used in the study of heavy fractions of petroleum (Karas and Hillenkamp, 1988). Because this technique tends to use a laser intensity that is low enough to vaporise the compounds without breaking their covalent bounds, it is considered a "soft" mass spectrometric technique. Since the method is also used to analyse compounds that display low light absorption and therefore require the addition of a laser-absorbing matrix, it is often known as the matrix-assisted laser desorption ionisation (MALDI) mass spectrometry. In practice, for high laser-absorbing samples such as asphaltenes, matrices are found not to be necessary (Acevedo et al., 2005; Apicella et al., 2007; Martínez-Haya et al., 2007; Pantoja et al., 2013; Rizzi et al., 2006; Tanaka et al., 2004).

In the present contribution, asphaltenes extracted from an oil sand sample was fractionated using a binary solvent system. The chemical structures of the asphaltene sample, together with its four subfractions, were studied using ^{13}C NMR in combination with DEPT-135, a method reported in our previous work (Zheng et al., 2017). A set of average structural parameters, such as average polycyclic aromatic hydrocarbon (PAH) size, average side chain length and average molecular weight (AMW), were calculated based on the NMR and DEPT results. MALDI-TOF was also employed to measure the molecular weight distributions (MWDs) of the asphaltene sample and its subfractions, in order to assist the interpretation of the ^{13}C NMR spectra. It was expected that the combined use of the three techniques would provide further insights into the understanding of the structural differences of the subfractions and shed new light on the fractionation mechanisms of the asphaltenes in the binary solvent system.

2. Experimental

2.1 Materials and sample preparation

The asphaltene sample was extracted from Buton Oil Sand from Indonesia. The "run of mine" oil sand was crushed and pulverised into fine powders with sizes <200 μm. The crushed sample was then subjected to solvent extraction using toluene in a Soxhlet extractor to obtain the organic fraction. The asphaltenes were isolated from the organic fraction in accordance with the method prescribed by the ASTM D-3279. Briefly, a sample of the organic fraction of the oil sand was firstly subjected to Soxhlet extraction using *n*-heptane as the solvent for at least 48 hours until no discoloration was observed in the reflux. The extraction was then continued by replacing *n*-heptane with toluene as the solvent for a further period of at least 8 hours till no further discoloration. The final extract was filtered, evaporated to dryness at 40°C using a rotary evaporator and further dried at 100°C under vacuum in an electric oven. The asphaltene sample thus prepared, denoted as *Buton*, was collected in clean glass vials, sealed and stored in darkness before further characterisation and analysis.

The Buton asphaltene was subjected to fractionation following a procedure as illustrated in Figure 1. Briefly, the asphaltene sample was initially dissolved in DCM and stirred for 2 hours. A solvent-to-sample ratio of 80:1 by weight was used, which had proven to be sufficient to fully dissolve the sample in preliminary filtration trials prior to this research. Subsequently, *n*-heptane was slowly added into the solution under stirring to form a binary solvent with a volumetric ratio of DCM/*n*-heptane being 30/70. The mixture was left stirring for further 24 hours. The *first fraction* (F1), also known as the *least soluble fraction*, was recovered by filtering the mixture through Waterman GF/B glass microfiber filters, while the filtrate in the DCM/*n*-heptane solvent was evaporated in a rotary evaporator to recover the soluble fraction. For the subsequent fractions, the same separation procedure was repeated except the ratio of the binary solvent was in turn changed to 20/80 and 10/90. The insoluble fractions isolated from 20/80 and 10/90 were denoted as the *second fraction*

(F2) and *the third fraction* (F3), respectively. The soluble fraction from the last separation step was the *most soluble fraction* and was assigned as the *fourth fraction* (F4).

2.2 Characterisation and Analysis

The organic elemental compositions of the asphaltene sample and its fractions were acquired using a PerkinElmer 2400 Series II CHNS elemental analyser following ASTM D-5291. The analyses were repeated three times and the results are listed in Table 1.

The liquid ^{13}C NMR spectroscopy analyses were performed using a Varian 400 NMR spectrometer operating at 100.55 MHz. When preparing a sample for the NMR analysis, 80 mg of each asphaltene sample was dissolved in 0.8 ml of Deuterated chloroform ($CDCl_3$). Chromium acetylacetonate ($Cr(acac)_3$) was added into the solution at a concentration of 0.01M to ensure complete nuclear magnetic moment relaxation between pulses. In order to obtain quantitative results of ^{13}C NMR, the inverse gated decoupling technique was applied to suppress the Nuclear Overhauser Effect (NOE). The spectra were collected with a 45° flip angle, 1.05 seconds acquisition time, 6.50 seconds recycle delay, 24,510 Hz spectral width and 30,000 scans. $CDCl_3$ peaks at 77.16 ppm were employed as the reference.

The DEPT 135° (DEPT-135) spectroscopy analyses were performed with the same samples and the same Varian 400 NMR spectrometer, but operated using the following parameters: a polarisation transfer delay corresponding to J = 140 Hz and a relaxation delay of 6.50 seconds. To obtain sufficient signal-to-noise ratios, 7,500 scans were collected.

The MWDs of the asphaltene sample and the fractions were obtained using an Ultraflex III MALDI-TOF mass spectrometer (Bruker Daltonics, Bremen, Germany). Runs with/without a matrix were carried out in parallel to examine the effect of the matrix on the results. In the case of the matrix being employed, a solution of 90% v/v acetonitrile (ACN) and 10% v/v saturated α-cyano-4-hydroxycinnamic acid (CHCA) in TA90 solution (90% ACN, 0.01%TFA) were used as the matrix to disperse the asphaltene sample. For a typical run, 1 μl of 0.01 $mg \cdot ml^{-1}$ asphaltenes in a DCM solution was spotted on the plate. The sample was ionised in the positive ion mode. Spectra

were collected in the reflector mode with laser intensity in the range of 20% - 25% and upon accumulation of 1,000 shots. The detection range was from 0 to 4,000Da but the mass signals below m/z = 200 were suppressed to eliminate the background noise.

3. Results and Discussion

3.1 Fractionation Yield

The yields and the elemental analysis results for the subfraction samples are shown in Table 1, together with the calculated H/C ratios. The process loss was about 5% by weight, which was incurred during the recovery of F1. It was shown that oxygen enriched in the least soluble subfraction F1. The H/C ratios of the subfractions increased from F2 to F4, while which of F1 and Buton fell in between.

3.2 Aromaticity

An important structural parameter, the aromaticity (f_{ar}) was determined using ^{13}C NMR. This parameter has been used widely in the literature (Fergoug and Bouhadda, 2014; Luo et al., 2010; Ostlund et al., 2004; Sanchez-Minero et al., 2013) to gauge the aromatic fraction. Figure 2 shows typical ^{13}C NMR spectra of Buton and its subfractions. The ^{13}C NMR spectra were separated into the aromatic region from 100 to 160 ppm and the aliphatic region from 0 to 60 ppm. Based on this method, f_a can be calculated from Dickinson's equation (Dickinson, 1980; Knight, 1967):

$$f_a = \frac{C_{ar}}{C_{ar}+C_{al}} \quad (1)$$

where C_{ar} and C_{al} stand for the integrations of the aromatic region and the aliphatic region, respectively. The calculated f_a values are listed in Table 2.

As shown in Row 1 of Table 2, the aromaticity of Buton revealed as an average of the aromaticities of its four subfractions. The aromaticities of the subfractions followed an increasing order of F2 > F1 > F3 > F4, where the aromaticity of F1 (44.21) is similar to that of Buton (44.44). The H/C atomic ratios shown in Table 1 followed the same pattern.

3.3 Carbon types

As shown in Figure 2, the ^{13}C NMR spectra suffered severe overlaps in both the aromatic and aliphatic regions. In order to distinguish the different types of carbon, DEPT-135 analyses were performed. Figure 3 shows the typical DEPT-135 spectra of the asphaltene samples and Figure 4 shows their corresponding spectra in the aliphatic region with a chemical shift from 0 ppm to 60 ppm. As commonly known (Doddrell et al., 1982), CH and CH_3 peaks are shown facing upwards, in a direction opposite to that of the CH_2 in a DEPT spectrum Which could be used to help resolve overlapping peaks in aliphatic region of ^{13}C NMR spectra (Michon et al., 1997). As shown in Figure 4, the assignments of the regions representing different aliphatic carbons were determined with the help of corresponding DEPT-135 spectra. The assignments of the chemical shift regions for aliphatic carbons are summarised in Table 3.

However, it was still difficult to resolve the broad peaks in the aromatic region (100 to 160 ppm), as both the DEPT-135 and ^{13}C NMR spectra suffered from the overlap of both protonated and bridgehead carbons as shown in Figures 2 and Figure 3. In literature reports, the chemical shift regions of bridgehead carbon region was assigned up to 137 ppm (Masuda et al., 1996; Michon et al., 1997; Rafenomanantsoa et al., 1994; Yoshida et al., 1980), as it was believed that hetero aromatic rings and hydroxyl group could push the chemical shift of some bridgehead carbon as far as 137 ppm in spectra. Considering the relative rarity of hetero aromatic ring in asphaltenes, the upper limit of the bridgehead carbon region was assigned to 133 ppm as suggested by Artok el al (1999) and Andrews et al (2011). The signals of the protonated aromatic carbon appeared at the chemical shift ranging from 100 to 130 ppm, overlaying with the potential region of bridgehead carbon with the chemical shift ranging from 124 to 133 ppm. Some literature reports tend to simply define the two regions at a cut-off point of 126.5 ppm (Begon et al., 2003; Fergoug and Bouhadda, 2014; Masuda et al., 1996), that is, the chemical shift from 100 to 126.5 ppm was deemed to belong to the protonated aromatic carbon region and that from 126.5 to 133 ppm was regarded as the

bridgehead carbon region. This could be very biased and lead to a large deviation from the true composition of asphaltenes (Andrews et al., 2011).

In the present study, the method proposed by Andrews et al (2011) was adopted to determine the amount of protonated aromatic carbon using both DEPT-135 spectra and ^{13}C NMR spectra. Instead of using a cut-off point, the intensity of protonated aromatic carbon was mathematically determined and subtracted from the overlapping region. Briefly, the intensity ratio between paraffinic methyl carbon and protonated aromatic carbon in the DEPT spectrum, $CH_{3\%}/C_{pr\%}$ as shown in Table 3, was firstly obtained. In order to make sure $CH_{3\%}/C_{pr\%}$ is of quantitative significance, the ratio was further normalised considering the polarisation intensities for carbons with different number of protons attached, as described below (Friebolin and Becconsall, 1993):

CH: Signal Intensity $= [\gamma(^1H)/\gamma(^{13}C)] \sin\theta$;

CH_2: Signal Intensity $= [\gamma(^1H)/\gamma(^{13}C)] \sin 2\theta$;

CH_3: Signal Intensity $= [3\gamma(^1H)/4\gamma(^{13}C)] (\sin\theta+\sin 3\theta)$

where γ is the magnetogyric ratio of the nucleus and θ is the pulse angle. Then the $CH_{3\%}/C_{pr\%}$ ratio was applied to the ^{13}C NMR spectrum of the same sample to calculate the intensity of the protonated aromatic carbon in the overlapping region, using the intensity of paraffinic methyl carbon in the ^{13}C NMR spectrum. The assignments of the regions representing different aromatic carbons are also summarised in Table 3.

Based on the chemical shift regions defined in Table 3, the average percentages of various aliphatic carbon and aromatic carbon were calculated by integrating the corresponding peaks on the quantitative ^{13}C NMR spectra. The results are listed in Rows 2-11 of Table 2. It is evident that the percentage of phenolic aromatic carbon ($C_{phen\%}$, Row 11 in Table 3) in F1 was almost tripled in comparison to that of the other subfractions, which corresponded to a much higher oxygen content as shown in Table 1.

3.4 PAH size

After subtracting the intensity of the protonated carbon in the overlapping region (100 to 133 ppm), the percentage (X_b) of bridgehead carbon ($C_{br\%}$) to the total aromatic carbon ($C_{ar\%}$) was obtained. In order to estimate the average size of the PAH cores, the theory developed by Solum et al. (1989) was espoused in the present work, which established the connection between X_b and the number of aromatic carbon per PAH core (C_{ar}), as represented by:

$$X_b = \frac{1-\tanh(\frac{C_{ar}-C_0}{m})}{2} X_b' + \frac{1+\tanh(\frac{C_{ar}-C_0}{m})}{2} X_b'' \quad (2)$$

where C_0 and m are adjustable parameters to give the best fit of the dependence of X_b on C_{ar}; optimal values of $C_0 = 19.57$ and $m = 4.15$ were determined for all of the aromatic hydrocarbons projecting on to Coronene; X_b' $(1/2 - 3/C_{ar})$ and X_b'' $(1 - \sqrt{6}/\sqrt{C_{ar}})$ represent the molar fractions of the bridgehead carbon in catacondensation and in pericondensation (Solum et al., 1989).

The calculated X_b and C_{ar} values for Buton and its subfractions are listed in Row 12-13 of Table 3. The X_b values obtained for Buton and its subfractions were roughly the same, except which for F1, as shown in Row 12 of Table 3. The C_{ar} obtained as shown in Row 13 of Table 3 showed that the differences among the subfractions were less than two carbons, indicating roughly the same average PAH size.

3.5 Molecular architecture

From the average numbers of aromatic carbon (C_{ar}) estimated as shown in Row 13 of Table 2, an average PAH size of 5 or 6 rings was estimated for Buton and most of its subfractions (F2 to F4) depending on the type of condensation. The average PAH size for F1 could be 6 or 7 rings, slightly larger than those of the other fractions. In theory, the pericondensation is predominant when X_b is larger than 0.49 ($C_{ar} \geq 24$), while the catacondensation is the governing mechanism when X_b is smaller than 0.29 ($C_{ar} \leq 14$) (Solum et al., 1989). Considering asphaltenes are a group of different compounds containing PAH cores, the C_{ar} values of 22~24 for Buton and its subfractions indicated that an overwhelming majority of the mixed compounds were in the form of pericondensation. Thus it is believed that an average of 6 fused rings PAH in F2 to F4, and possibly a larger PAH core with

an average of 7 fused rings in F1 as a result of the two additional aromatic carbons. The average PAH size of Buton was, as a sum of its subfractions, 6 fused rings in the form of pericondensation. A great deal of literature publications have reported similar results on the molecular architecture of asphaltenes isolated from both coal and petroleum (Andrews et al., 2011; Groenzin and Mullins, 1999; Groenzin and Mullins, 2000, 2007, 2010; Mullins et al., 2012). However, the detailed PAH structures of asphaltenes are very complicated. There was a high level of heteroatoms such as oxygen and sulphur, in the asphaltenes, which could present in aromatic rings as furan and thiophene.

In order to further examine the average molecular architecture for the asphaltene samples, based on C_{ar}, f_a and $C_{sub\%}$ (as defined in Table 3), the average number of aliphatic substitutions per PAH core (n_{sub}) and the total number of the aliphatic and aromatic carbons (C) were calculated using the following equations:

$$n_{sub} = (C_{sub\%}/f_a) \times C_{ar} \quad (3)$$

$$C = C_{ar}/f_a \quad (4)$$

Knowing C and n_{sub}, the average number of aliphatic carbon per cluster (C_{al}) and the average carbon number per alkyl chain (N) were calculated as follows:

$$C_{al} = (1 - f_a) \times C \quad (5)$$

$$N = C_{al}/n_{sub} \quad (6)$$

The calculated results are listed in Rows 14-17 in Table 2.

It is noted that the average molecular parameters obtained from the NMR spectra followed a monotonic increasing or decreasing trend from F2 to F4. F1 was incongruous in the rows which will be discussed in the following paragraphs. From F2 to F4, the aliphatic parts became larger while the sizes of PAH cores stayed the same (Row 16 and Row 13 in Table 2) in an “average molecules”, while the degree of aliphatic substitution on the PAH changed marginally (Row 14 in Table 2). As a result, the average chain length of the aliphatic substitution increased significantly from 2.90 to 3.96 as shown in Row 17 of Table 2.

Hypothetically, the asphaltene molecules were attracted together as a result of π-π stacking through the PAH cores while this attractive forces were offset by repulsive forces generated from the aliphatic substituents (Hashmi and Firoozabadi, 2013; Mullins, 2010; Mullins et al., 2012). The intermolecular forces amongst the asphaltene compounds in each fraction must be attractive and greater than the "pulling-apart" capability of the particular binary solvent system (Mullins, 2010). In other words, the fractionation of Buton in the DCM/*n*-heptane binary solvent system was achieved by sorting the asphaltene molecules with different levels of "net intermolecular attractive force". In the present study, the "net intermolecular attractive force" was found to be determined primarily by the luxuriance of the aliphatic part, as the PAH sizes were roughly the same across the subfractions.

As the least soluble fraction in this binary solvent system, F1 was expected to show the highest aromaticity, or in other words the highest "net intermolecular attractive force". However, the calculation results from NMR showed that F1 defied the trend observed in F2 to F4. It could be a result of the notably high heteroatom contents found in F1 as shown in Table 1. Sulphur and oxygen could potentially promote intermolecular bonding, which favoured aggregation (Foster, 1974; Murgich, 2002; Murgich et al., 1996) and therefore made some compounds precipitate in F1 with relatively lower aromaticity. More importantly, the compounds in F1 could be much more polarised than the ones in the other fractions due to the presence of some functional groups, such as hydroxyl, carboxylic and thiol. The presence of these functional groups would make the compounds too polar to stay in a nonpolar solvent, therefore precipitation happened as soon as *n*-heptane was added into the system. The high abundance of phenolic aromatic carbon in F1 as shown in Row 11 of Table 2 provided the evidence for the existence of hydroxyl groups. As these functional groups could be present in the asphaltene molecules with any type or size, the average molecular parameters of F1, not surprisingly, were similar to those of Buton as clearly shown in Table 2. It is believed that a portion of the compounds in F1 was precipitated following the "net intermolecular attractive force" theory as discussed previously, and consequently showing a relatively larger average PAH size and

the shortest average substitution length; the other part of the compounds in F1 was precipitated due to the presence of polar functional groups, thus some of the average molecular parameters seemed "abnormal" in the group of subfractions. Leaving F1 aside, the average molecular parameters from F2 to F4 followed either an increasing or a decreasing pattern which was in consistence with the hypothesis of the "net intermolecular attractive force" theory.

Furthermore, there was a roughly 5 wt% loss during the fractionation process. It mainly happened during the course of recovering F1 from the glassfibre filter paper, as the isolated F1 did not completely dissolve back into the solution. In the solubility tests, the DCM solution with the same asphaltene concentration had left nothing on filters, which eliminates the possibility that asphaltenes were not fully dissolved at the very beginning. Other researchers have reported similar observations in the past (Andersen et al., 1997; Nalwaya et al., 1999), arguing that precipitation of asphaltenes was not a reversible process. Hirschberg et al. (1984) suggested that the process is reversible but very slow. In fact, even boiling toluene in which Buton was initially isolated, was not able to dissolve the insoluble residue on filter paper. This clearly indicated that the intermolecular forces had changed amongst those insoluble molecules, or micelles as some researcher reported (Andreatta et al., 2005). The hypothesis is that the fractionation process weakened the "peptising" or "facilitating" effect to those "heavy" molecules in F1, by removing the "light" molecules in F3 and F4. With the help of "light" molecules, DCM or toluene was able to keep the "heavy" molecules away from each other, thus stay in solution. The intermolecular interactions amongst the "heavy" molecules once formed are too strong for DCM, and thus the re-dissolution is impractical or at least very time-consuming. The 5 wt% loss may contain molecules with much higher aromaticity and would potentially be categorised as a part of F1 if they had been managed to re-dissolve in the solution.

3.6 Molecular weight

363 Based on the assumption that only one PAH core existed in each molecule (Groenzin and Mullins,
364 1999, 2000; Mullins, 2007, 2010, 2011; Sabbah et al., 2011), the numbers of other atoms, namely
365 H, N, S and O, were calculated according to the organic elemental analyses shown in Table 1. The
366 AMWs were computed as the sums of the atomic weights of all the elements in the given samples.
367 The results are shown in Rows 18-22 of Table 2. In order to determine the number of PAH in an
368 average asphaltene molecule and validate the AMWs calculated from the data derived from the
369 NMR/DEPT spectra, the AMWs of Buton and its subfractions were calculated using MALDI-TOF.
370 The typical MWDs of the samples measured using MALDI-TOF are shown in Figure 5. In
371 consistence with the previous observations (Acevedo et al., 2005; Apicella et al., 2007; Martínez-
372 Haya et al., 2007; Pantoja et al., 2013; Rizzi et al., 2006; Tanaka et al., 2004), no difference was
373 found between the spectra obtained with and without a matrix. The results presented here were
374 therefore obtained without the use of a conventional matrix and based on the asphaltene own "self-
375 matrix" propensity. As shown in Figure 5, the samples had similar MWD profiles at the same
376 intensity scale. It may be also seen that the majority of the detectable masses were present under the
377 1,500-m/z range, although there were "grass peaks" visible in the region up to 3,000m/z in F1 and
378 F2.
379 The MWDs of the samples can provide information necessary to help with understanding of the
380 architecture of the asphaltene molecules, such as the number of PAH in an average asphaltene
381 molecule. Based on the MWDs of the samples, the AMW values may be derived from the following
382 equation (Hurt et al., 2013):

383 $$AMW = \frac{\sum[(\frac{m}{z})\times A_i]}{\sum A_i} \quad (7)$$

384 where A_i stands for the intensity of the individual peaks (*1, 2, 3, …, i*) in the MWD spectrum, and *z*
385 is the charge. Since MALDI mainly generates single-charged species, *z* is always equal to 1 in this
386 case. Thus we use "Dalton (Da)", instead of "m/z", in the following elucidation.
387 From Equation (7), it is evident that the AMW calculation is dependent on the summation range.
388 There were practically no peaks observed beyond the 3,000Da limit and hence the AMW values

were calculated respectively in four summation ranges, namely 0–1,000Da, 0–1,500Da, 0–2,000Da and 0–3,000Da. The results are shown in Table 4, together with the AMW values derived from the NMR spectra for comparison.

The AMWs derived from MALDI-TOF revealed the same pattern as estimated from the NMR spectra. The AMWs deceased from F1 to F2 and then increased from F2 to F4 regardless of the summation range, except in the range 0–1,000Da where the AMWs constantly increased from F1 to F4 probably due to exclusion of some large molecules. Although the results in Table 4 become slightly larger as the summation range increases, each putative molecular weight in every range may only fit one PAH cluster. This confirms that each molecule contains only one PAH core, thus reassures the validity of the combined NMR/DEPT method in estimating the structural parameters of asphaltenes. In other words, the island molecular architecture is predominant in all the asphaltene samples studied. This is in consistence with previous studies of coal-derived and petroleum asphaltenes using various techniques such as time-resolved fluorescence depolarisation and two-step laser desorption ionisation (Groenzin and Mullins, 1999; Mullins, 2007, 2010; Sabbah et al., 2011).

4. Conclusions

In the present work, an oil sand asphaltene sample was fractionated into four subfractions using the DCM/*n*-heptane binary solvent system. The combination of NMR/DEPT and MALDI-TOF allowed the chemical structure of the oil sand and its subfractions to be revealed.

F1, the least soluble fraction, was found to contain an extremely high amount of oxygen. The average PAH size of F1 was about 7 fused rings in the form of pericondensation, while the other subfractions, F2 to F4, were found to contain an average PAH size of 6 rings dominated by pericondensation as well. The island architecture was shown to be predominant across the oil sand asphaltene sample and its subfractions.

414 The AMWs of the samples were found to be <1000 Da. The AMW increased from F2 to F4, while
415 that of F1 fell in between. The precipitation mechanism was dictated by the compound polarity. The
416 most polar compounds precipitated in F1 while the remaining ones precipitated sequentially from
417 F2 to F4 according to relative “lushness” of their aliphatic parts. The average molecular parameters
418 of the oil sand asphaltene sample were shown to represent an average of its subfractions.
419
420

421 Acknowledgement

422 Partial financial support has been received from the Australian Research Council under the ARC
423 Discovery Projects (ARC DP160103636) and Linkage Projects Scheme (ARC LP100200135 and
424 ARC LP100200136). The authors acknowledge the access to the analytical and characterisation
425 facilities and associated scientific and technical assistance provided by the Australian Microscopy
426 and Microanalysis Research Facility at the Centre for Microscopy, Characterisation and Analysis,
427 The University of Western Australia (UWA), a facility funded by the University, State and
428 Commonwealth Governments. Ce Zheng also acknowledges the University Postgraduate Awards
429 scholarship provided by UWA.
430

References

Acevedo, S., Gutierrez, L. B., Negrin, G., Pereira, J. C., Mendez, B., Delolme, F., Dessalces, G., Broseta, D. 2005. Molecular weight of petroleum asphaltenes: a comparison between mass spectrometry and vapor pressure osmometry. Energy Fuels 19(4), 1548-1560.

Ancheyta, J., Trejo, F., Rana, M. S. 2010. Asphaltenes: chemical transformation during hydroprocessing of heavy oils, CRC press.

Andersen, S. I., Keul, A., Stenby, E. 1997. Variation in composition of subfractions of petroleum asphaltenes. Pet. Sci. Technol. 15(7-8), 611-645.

Andreatta, G., Bostrom, N., Mullins, O. C. 2005. High-Q ultrasonic determination of the critical nanoaggregate concentration of asphaltenes and the critical micelle concentration of standard surfactants. Langmuir 21(7), 2728-2736.

Andrews, A. B., Edwards, J. C., Pomerantz, A. E., Mullins, O. C., Nordlund, D., Norinaga, K. 2011. Comparison of coal-derived and petroleum asphaltenes by ^{13}C nuclear magnetic resonance, DEPT, and XRS. Energy Fuels 25(7), 3068-3076.

Apicella, B., Carpentieri, A., Alfè, M., Barbella, R., Tregrossi, A., Pucci, P., Ciajolo, A. 2007. Mass spectrometric analysis of large PAH in a fuel-rich ethylene flame. Proc. Combust. Inst. 31(1), 547-553.

Artok, L., Su, Y., Hirose, Y., Hosokawa, M., Murata, S., Nomura, M. 1999. Structure and reactivity of petroleum-derived asphaltene. Energy & Fuels 13(2), 287-296.

Begon, V., Suelves, I., Islas, C. A., Millan, M., Dubau, C., Lazaro, M. J., Law, R. V., Herod, A. A., Dugwell, D. R., Kandiyoti, R. 2003. Comparison of the quaternary aromatic carbon contents of a coal, a coal extract, and its hydrocracking products by NMR methods. Energy Fuels 17(6), 1616-1629.

Buch, L., Groenzin, H., Buenrostro-Gonzalez, E., Andersen, S. I., Lira-Galeana, C., Mullins, O. C. 2003. Molecular size of asphaltene fractions obtained from residuum hydrotreatment. Fuel 82(9), 1075-1084.

457 Buenrostro-Gonzalez, E., Andersen, S. I., Garcia-Martinez, J. A., Lira-Galeana, C. 2002.
458 Solubility/molecular structure relationships of asphaltenes in polar and nonpolar media.
459 Energy Fuels 16(3), 732-741.
460 Buenrostro-Gonzalez, E., Groenzin, H., Lira-Galeana, C., Mullins, O. C. 2001. The overriding
461 chemical principles that define asphaltenes. Energy Fuels 15(4), 972-978.
462 Calemma, V., Iwanski, P., Nali, M., Scotti, R., Montanari, L. 1995. Structural characterization of
463 asphaltenes of different origins. Energy Fuels 9(2), 225-230.
464 Christopher, J., Sarpal, A. S., Kapur, G. S., Krishna, A., Tyagi, B. R., Jain, M. C., Jain, S. K.,
465 Bhatnagar, A. K. 1996. Chemical structure of bitumen-derived asphaltenes by nuclear
466 magnetic resonance spectroscopy and X-ray diffractometry. Fuel 75(8), 999-1008.
467 Clutter, D. R., Petrakis, L., Stenger Jr, R. L., Jensen, R. K. 1972. Nuclear magnetic resonance
468 spectrometry of petroleum fractions. Carbon-13 and proton nuclear magnetic resonance
469 characterizations in terms of average molecule parameters. Anal. Chem. 44(8), 1395-1405.
470 Dickie, J. P., Yen, T. F. 1967. Macrostructures of the asphaltic fractions by various instrumental
471 methods. Anal. Chem. 39(14), 1847-1852.
472 Dickinson, E. M. 1980. Structural comparison of petroleum fractions using proton and 13C nmr
473 spectroscopy. Fuel 59(5), 290-294.
474 Doddrell, D. M., Pegg, D. T., Bendall, M. R. 1982. Distortionless enhancement of NMR signals by
475 polarization transfer. J. Magn. Reson. 48(2), 323-327.
476 Fergoug, T., Bouhadda, Y. 2014. Determination of Hassi Messaoud asphaltene aromatic structure
477 from ^{1}H & ^{13}C NMR analysis. Fuel 115(0), 521-526.
478 Foster, R. 1974. Organic charge transfer complexes, 1969. London, New York: Academic Press, R.
479 Foster (ed.), Molecular Complexes 73, 1-2.
480 Friebolin, H., Becconsall, J. K. 1993. Basic one-and two-dimensional NMR spectroscopy, VCH
481 Weinheim.

Gillet, S., Delpuech, J., Valentin, P., Escalier, J. 1980. Optimum conditions for crude oil and petroleum product analysis by carbon-13 nuclear magnetic resonance spectrometry. Anal. Chem. 52(6), 813-817.

Groenzin, H., Mullins, O. C. 1999. Asphaltene molecular size and structure. J. Phys. Chem. A 103(50), 11237-11245.

Groenzin, H., Mullins, O. C. 2000. Molecular size and structure of asphaltenes from various sources. Energy Fuels 14(3), 677-684.

Groenzin, H., Mullins, O. C., Eser, S., Mathews, J., Yang, M.-G., Jones, D. 2003. Molecular size of asphaltene solubility fractions. Energy Fuels 17(2), 498-503.

Hashmi, S. M., Firoozabadi, A. 2013. Self-assembly of resins and asphaltenes facilitates asphaltene dissolution by an organic acid. J. Colloid Interface Sci. 394, 115-123.

Hirschberg, A., DeJong, L. N. J., Schipper, B. A., Meijer, J. G. 1984. Influence of temperature and pressure on asphaltene flocculation. Society of Petroleum Engineers Journal 24(03), 283-293.

Hurt, M. R., Borton, D. J., Choi, H. J., Kenttämaa, H. I. 2013. Comparison of the structures of molecules in coal and petroleum asphaltenes by using mass spectrometry. Energy Fuels 27(7), 3653-3658.

Jacobs, F. S., Filby, R. H. 1983. Liquid chromatographic fractionation of oil-sand and crude oil asphaltenes. Fuel 62(10), 1186-1192.

Kaminski, T. J., Fogler, H. S., Wolf, N., Wattana, P., Mairal, A. 2000. Classification of asphaltenes via fractionation and the effect of heteroatom content on dissolution kinetics. Energy Fuels 14(1), 25-30.

Karas, M., Hillenkamp, F. 1988. Laser desorption ionization of proteins with molecular masses exceeding 10,000 daltons. Anal. Chem. 60(20), 2299-2301.

Knight, S. A., 1967. Analysis of aromatic petroleum fractions by means of absorption mode carbon-13 NMR spectroscopy, Chem. Ind. 11, 1920–1923.

508 Korb, J.-P., Louis-Joseph, A., Benamsili, L. 2013. Probing structure and dynamics of bulk and
509 confined crude oils by multiscale NMR spectroscopy, diffusometry, and relaxometry. J.
510 Phys. Chem. B 117(23), 7002-7014.
511 Luo, P., Wang, X., Gu, Y. 2010. Characterization of asphaltenes precipitated with three light
512 alkanes under different experimental conditions. Fluid Phase Equilib. 291(2), 103-110.
513 Martínez-Haya, B., Hortal, A. R., Hurtado, P., Lobato, M. D., Pedrosa, J. M. 2007. Laser
514 desorption/ionization determination of molecular weight distributions of polyaromatic
515 carbonaceous compounds and their aggregates. J. Mass Spectrom. 42(6), 701-713.
516 Masuda, K., Okuma, O., Nishizawa, T., Kanaji, M., Matsumura, T. 1996. High-temperature NMR
517 analysis of aromatic units in asphaltenes and preasphaltenes derived from Victorian brown
518 coal. Fuel 75(3), 295-299.
519 Michon, L., Martin, D., Planche, J.-P., Hanquet, B. 1997. Estimation of average structural
520 parameters of bitumens by ^{13}C nuclear magnetic resonance spectroscopy. Fuel 76(1), 9-15.
521 Mullins, O. C. 2010. The modified Yen model. Energy Fuels 24, 2179-2207.
522 Mullins, O. C. 2011. The asphaltenes. Annual Review of Anal. Chem., Vol 4. R. G. Cooks and E. S.
523 Yeung. 4: 393-418.
524 Mullins, O. C., Eric Y.; Hammami, Ahmed; Marshall, Alan G; 2007. Asphaltenes, Heavy Oils, and
525 Petroleomics, Springer, New York.
526 Mullins, O. C., Sabbah, H., Eyssautier, J., Pomerantz, A. E., Barre, L., Andrews, A. B., Ruiz-
527 Morales, Y., Mostowfi, F., McFarlane, R., Goual, L., Lepkowicz, R., Cooper, T., Orbulescu,
528 J., Leblanc, R. M., Edwards, J., Zare, R. N. 2012. Advances in asphaltene science and the
529 Yen-Mullins model. Energy Fuels 26(7), 3986-4003.
530 Murgich, J. 2002. Intermolecular forces in aggregates of asphaltenes and resins. Pet. Sci. Technol.
531 20(9-10), 983-997.
532 Murgich, J., Rodríguez, J., Aray, Y. 1996. Molecular recognition and molecular mechanics of
533 micelles of some model asphaltenes and resins. Energy Fuels 10(1), 68-76.

534 Myhr, M. B., Schou, L., Skjetne, T., Krane, J. 1990. Characterization of asphaltenes and co-
535 precipitated material from a Californian crude oil. Org. Geochem. 16(4–6), 931-941.
536 Nalwaya, V., Tantayakom, V., Piumsomboon, P., Fogler, S. 1999. Studies on asphaltenes through
537 analysis of polar fractions. Ind. Eng. Chem. Res. 38(3), 964-972.
538 Netzel, D. A. 1987. Quantitation of carbon types using DEPT/QUAT NMR pulse sequences:
539 application to fossil-fuel-derived oils. Anal. Chem. 59(14), 1775-1779.
540 Ostlund, J. A., Wattana, P., Nyden, M., Fogler, H. S. 2004. Characterization of fractionated
541 asphaltenes by UV-vis and NMR self-diffusion spectroscopy. J. Colloid Interface Sci.
542 271(2), 372-380.
543 Ovalles, C., Rogel, E., Moir, M., Thomas, L., Pradhan, A. 2012. Characterization of heavy crude
544 oils, their fractions, and hydrovisbroken products by the asphaltene solubility fraction
545 method. Energy Fuels 26(1), 549-556.
546 Pantoja, P. A., Mendes, M. A., Nascimento, C. A. O. 2013. Contribution of mass spectrometry in
547 assessing quality of petroleum fractions: the use of mass spectrometry for assessing
548 asphaltenes. J. Pet. Sci. Eng. 109(0), 198-205.
549 Petrova, L. M., Abbakumova, N. A., Zaidullin, I. M., Borisov, D. N. 2013. Polar-solvent
550 fractionation of asphaltenes from heavy oil and their characterization. Petroleum Chemistry
551 53(2), 81-86.
552 Rafenomanantsoa, A., Nicole, D., Rubini, P., Lauer, J. C. 1994. Structural analysis by NMR and
553 FIMS of the tar-sand bitumen of Bemolanga (Malagasy). Energy Fuels 8(3), 618-628.
554 Rizzi, A., Cosmina, P., Flego, C., Montanari, L., Seraglia, R., Traldi, P. 2006. Laser
555 desorption/ionization techniques in the characterization of high molecular weight oil
556 fractions. Part 1: asphaltenes. J. Mass Spectrom. 41(9), 1232-1241.
557 Sabbah, H., Morrow, A. L., Pomerantz, A. E., Zare, R. N. 2011. Evidence for island structures as
558 the dominant architecture of asphaltenes. Energy Fuels 25(4), 1597-1604.

559 Sanchez-Minero, F., Ancheyta, J., Silva-Oliver, G., Flores-Valle, S. 2013. Predicting SARA
560 composition of crude oil by means of NMR. Fuel 110, 318-321.
561 Sheremata, J. M., Gray, M. R., Dettman, H. D., McCaffrey, W. C. 2004. Quantitative molecular
562 representation and sequential optimization of Athabasca asphaltenes. Energy Fuels 18(5),
563 1377-1384.
564 Snape, C. E., Ladner, W. R., Bartle, K. D. 1979. Survey of carbon-13 chemical shifts in aromatic
565 hydrocarbons and its application to coal-derived materials. Anal. Chem. 51(13), 2189-2198.
566 Solum, M. S., Pugmire, R. J., Grant, D. M. 1989. Carbon-13 solid-state NMR of Argonne-premium
567 coals. Energy Fuels 3(2), 187-193.
568 Storm, D. A., Edwards, J. C., DeCanio, S. J., Sheu, E. Y. 1994. Molecular representations of Ratawi
569 and Alaska North slope asphaltenes based on liquid-and solid-state NMR. Energy Fuels
570 8(3), 561-566.
571 Tanaka, R., Sato, S., Takanohashi, T., Hunt, J. E., Winans, R. E. 2004. Analysis of the molecular
572 weight distribution of petroleum asphaltenes using laser desorption-mass spectrometry.
573 Energy Fuels 18(5), 1405-1413.
574 Tojima, M., Suhara, S., Imamura, M., Furuta, A. 1998. Effect of heavy asphaltene on stability of
575 residual oil. Catal. Today 43(3–4), 347-351.
576 Trejo, F., Ancheyta, J., Morgan, T. J., Herod, A. A., Kandiyoti, R. 2007. Characterization of
577 asphaltenes from hydrotreated products by SEC, LDMS, MALDI, NMR, and XRD. Energy
578 Fuels 21(4), 2121-2128.
579 Trejo, F., Centeno, G., Ancheyta, J. 2004. Precipitation, fractionation and characterization of
580 asphaltenes from heavy and light crude oils. Fuel 83(16), 2169-2175.
581 Wiehe, I. A., Liang, K. S. 1996. Asphaltenes, resins, and other petroleum macromolecules. Fluid
582 Phase Equilib. 117(1–2), 201-210.
583 Yang, M.-G., Eser, S. 1999. Fractionation and molecular analysis of a vacuum residue asphaltenes.
584 Papers of the Amer. Chem. Soc. 218, 625.

585 Yoshida, T., Maekawa, Y., Uchino, H., Yokoyama, S. 1980. Derivation of structural parameters for
586 coal-derived oil by carbon-13 nuclear magnetic resonance spectrometry. Anal. Chem. 52(6),
587 817-820.
588 Zheng, C., Zhu, M., Zhou, W., Zhang, D. 2017. A preliminary investigation into the
589 characterization of asphaltenes extracted from an oil sand and two vacuum residues from
590 petroleum refining using nuclear magnetic resonance, DEPT, and MALDI-TOF. ASME J.
591 Energy Resour. Technol. 139(3), 032905.
592
593
594
595
596
597
598
599
600
601
602
603
604
605
606
607
608
609
610

611 **Figure Captions**

612 Figure 1 A schematic illustration of the fractionation procedure

613 Figure 2 Typical ^{13}C NMR spectra of Buton and its subfractions

614 Figure 3 DEPT-135 spectra of Buton and its subfractions

615 Figure 4 Subdivision of the aliphatic regions according to DEPT-135

616 Figure 5 MALDI-TOF spectra of Buton and its subfractions

617

618

619 Figure 1

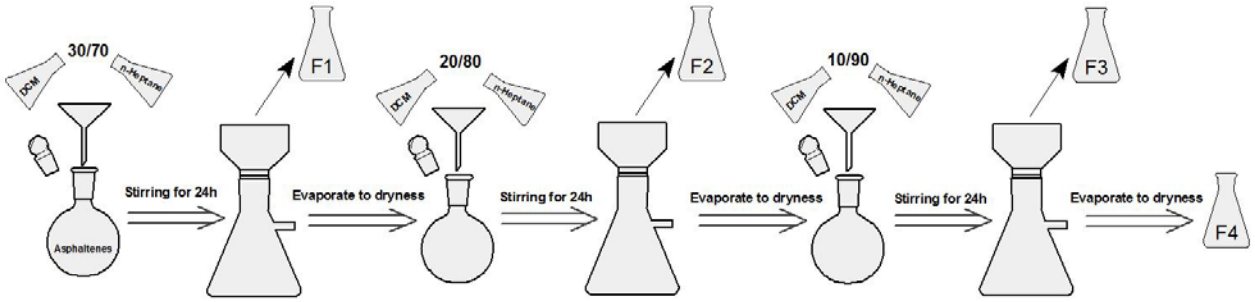

620

621 Figure 1 A schematic illustration of the fractionation procedure

622

623

624 Figure 2

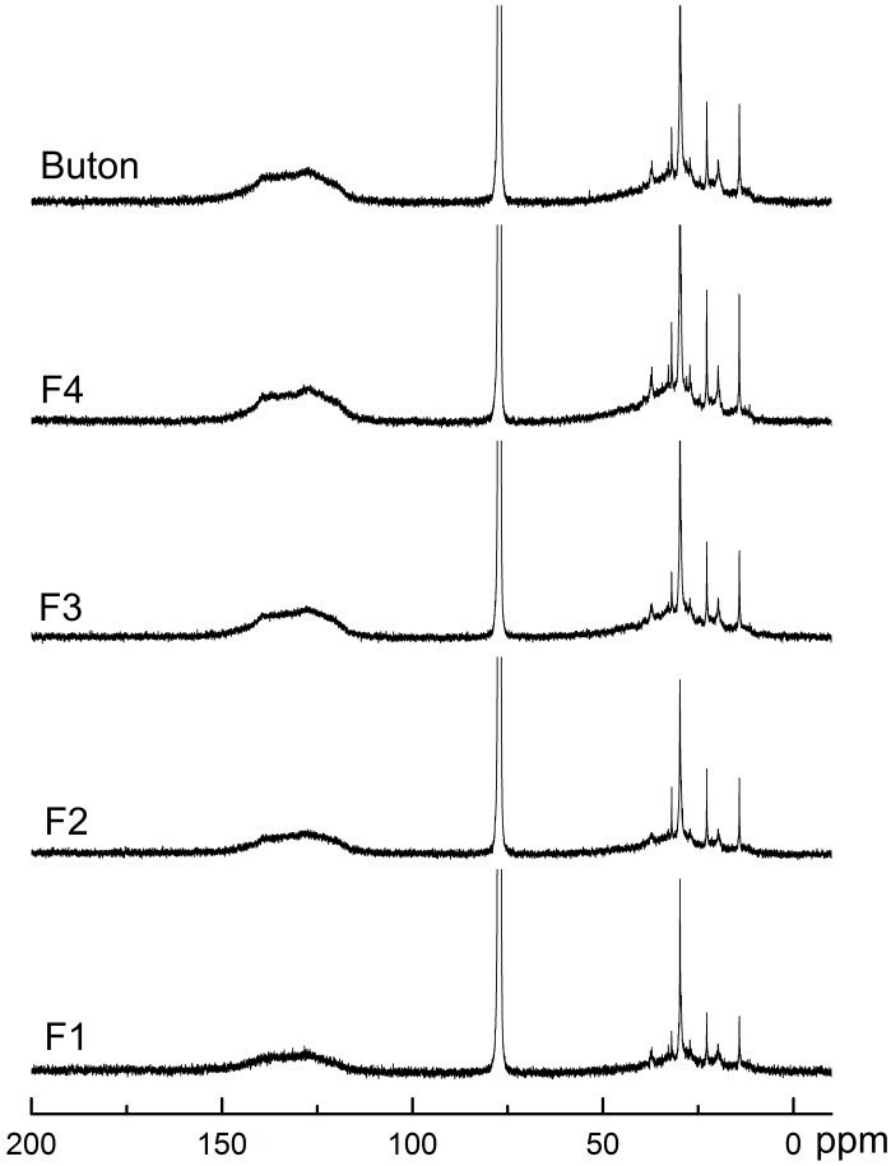

625

626 Figure 2 Typical ^{13}C NMR spectra of Buton and its subfractions

627

628

629 Figure 3

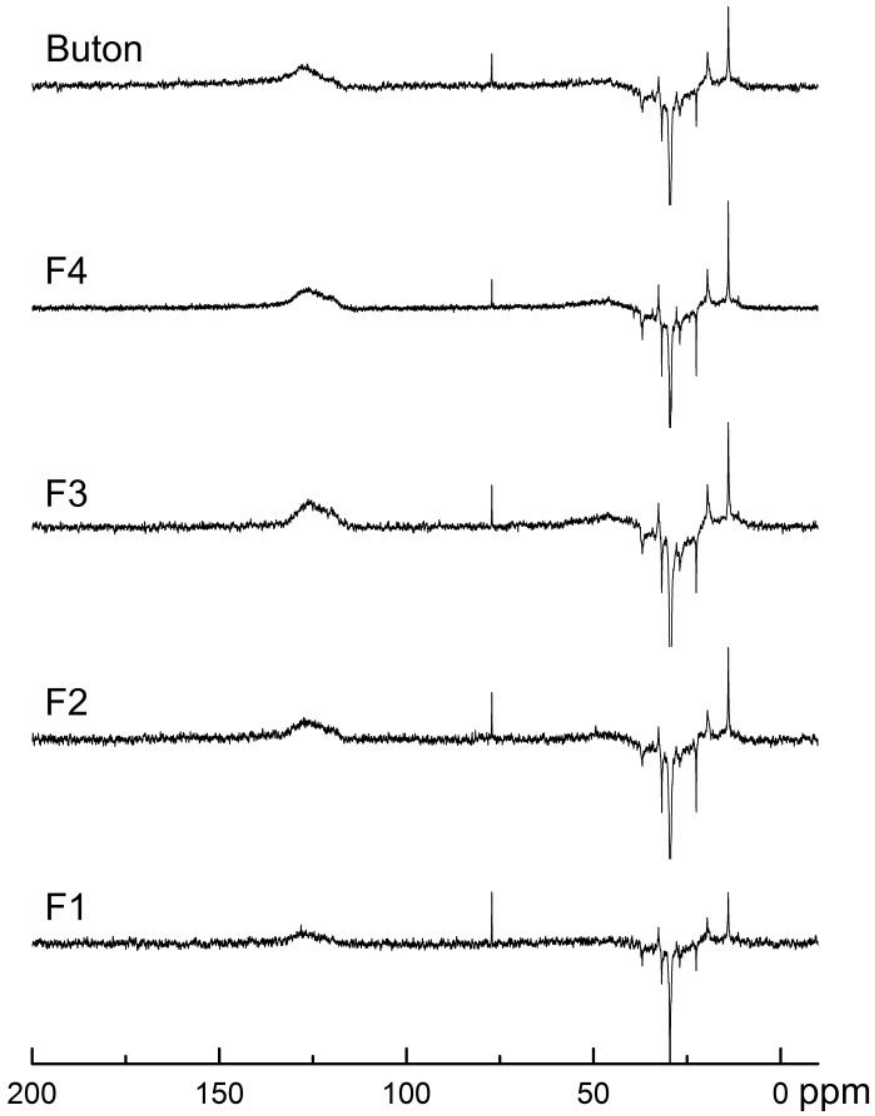

630

631 Figure 3 DEPT-135 spectra of Buton and its subfractions

632

633

634 Figure 4

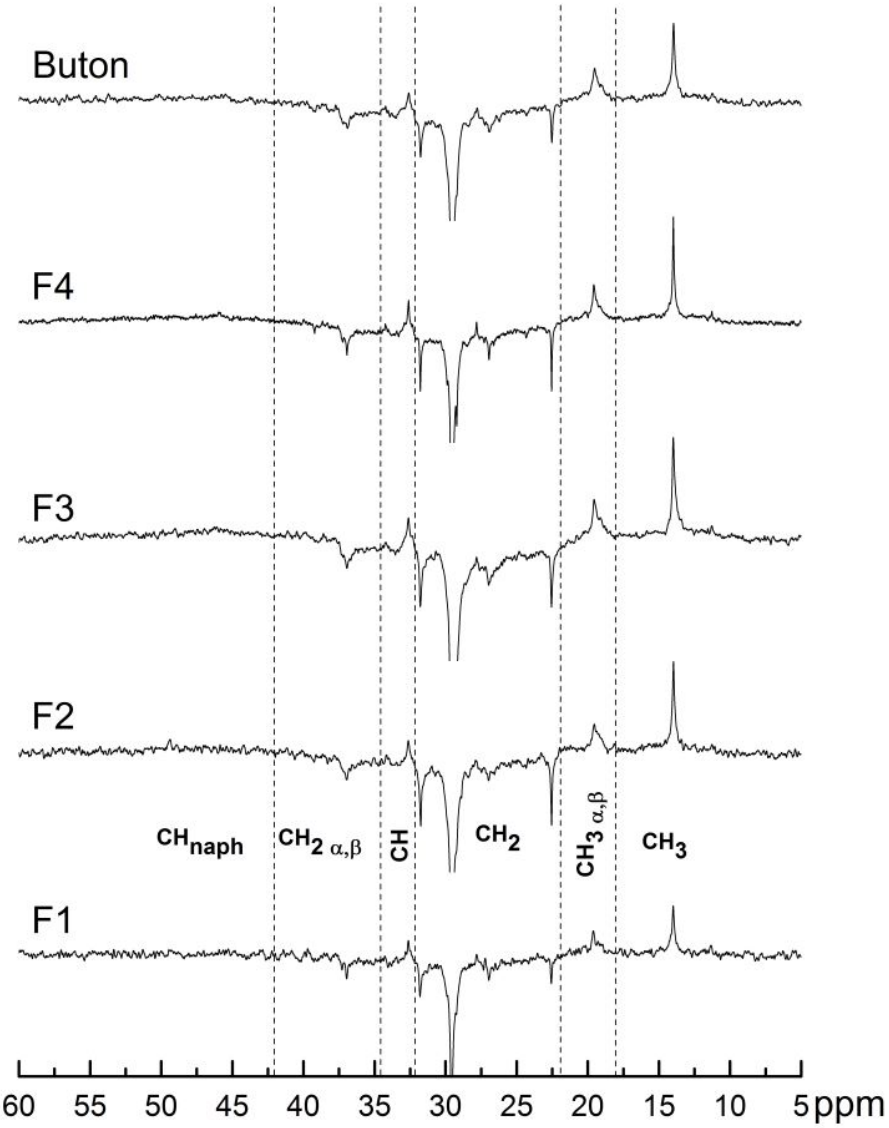

635

636 Figure 4 Subdivision of the aliphatic regions according to DEPT-135

637

638

639 Figure 5

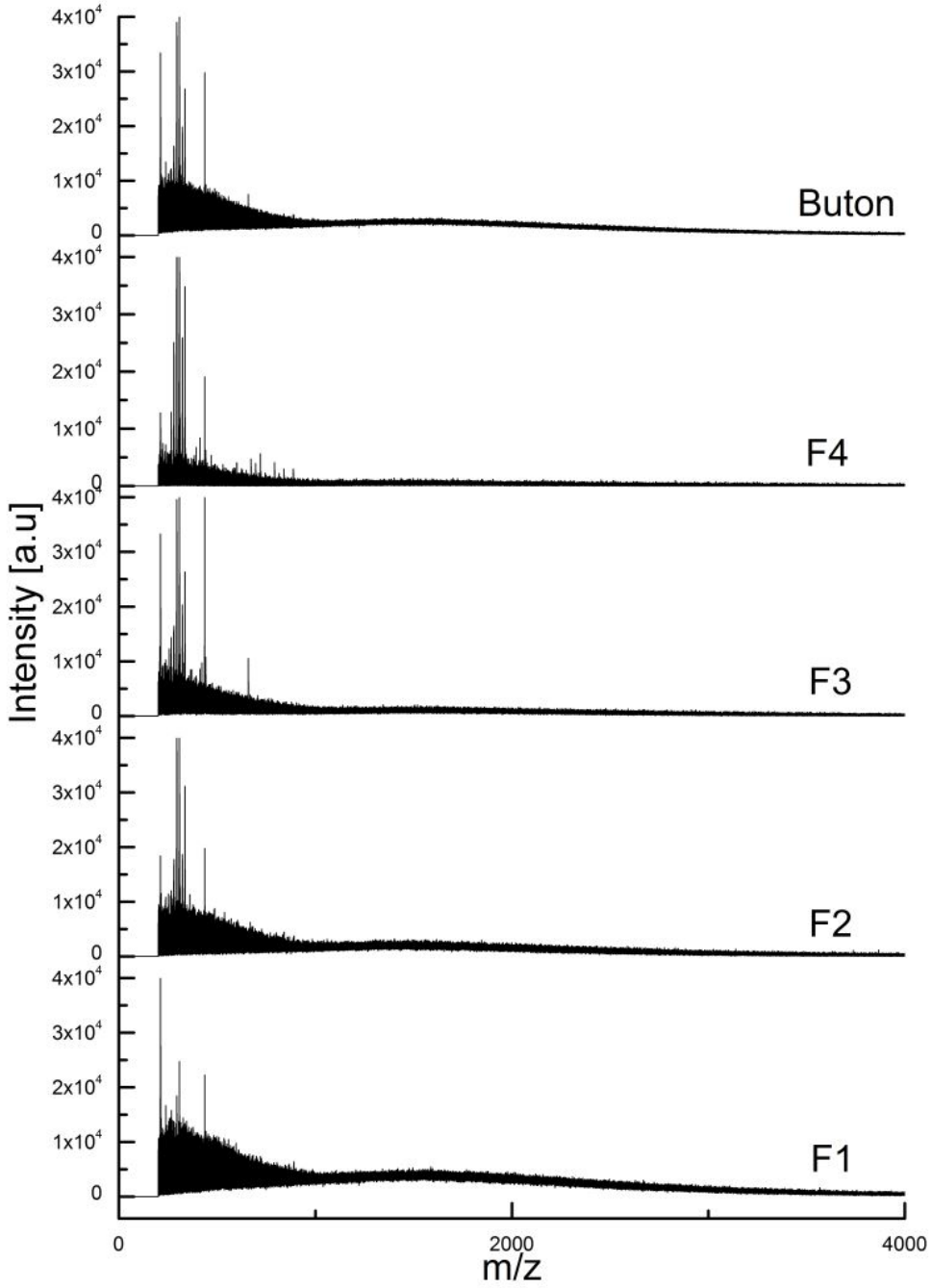

640

641 Figure 5 MALDI-TOF spectra of Buton and its subfractions

642

643

644 **List of Tables**

651

652

653 Table 1 Yields of the subfractions and their elemental compositions

	F1	F2	F3	F4	Buton	Loss
Fractionation yield (wt%)						
	28.56	12.42	20.08	33.92	N/A	5.02
Elemental composition (wt%)						
Carbon	72.11	77.62	79.27	79.85	75.06	N/A
Hydrogen	8.57	9.02	9.50	10.02	8.87	N/A
Nitrogen	0.89	0.96	0.91	0.85	0.90	N/A
Sulphur	7.66	8.71	8.51	8.04	8.13	N/A
Oxygen (by difference)	10.77	3.69	1.81	1.24	7.04	N/A
H/C atomic ratio	1.43	1.39	1.44	1.51	1.42	N/A

654

655

656

Table 2 Average structural parameters of Buton and its subfractions, calculated from ^{13}C NMR and DEPT-135 spectra

Row	Average Molecular Parameters*	F1	F2	F3	F4	Buton
1	*Aromaticity from ^{13}C NMR (f_a) %*	44.21	47.49	42.12	39.76	44.44
2	*Terminal methyl group $CH_{3\%}$*	7.68	4.85	6.90	5.59	6.25
3	*Methyl group at α or β position $CH_{3\ \alpha,\beta\%}$*	6.09	4.68	5.27	5.07	5.35
4	*Methylene group $CH_{2\%}$*	28.22	25.51	25.65	27.00	26.17
5	*Methine group $CH_{\%}$*	4.61	4.82	4.82	5.50	4.76
6	*Methylene group at α or β position CH_2*	7.64	9.16	9.33	10.76	9.06
7	*Methine group in naphthenic rings*	0.52	3.49	5.91	6.32	3.98
8	*Protonated/hetero aromatic $C_{pr\%}$*	1.73	7.19	5.46	6.16	4.68
9	*Bridgehead aromatic $C_{br\%}$*	21.44	21.42	19.08	17.97	20.13
10	*Substituted aromatic $C_{sub\%}$*	20.23	18.08	16.88	15.21	18.40
11	*Phenolic aromatic $C_{phen\%}$*	1.84	0.79	0.69	0.42	1.23
12	*Percentage of bridgehead carbon X_b*	0.485	0.451	0.453	0.452	0.453
13	*Average aromatic PAH size C_{ar}*	23.89	22.01	22.11	22.06	22.11
14	*Substitutions per PAH n_{sub}*	10.93	8.38	8.86	8.44	9.15
15	*Molecular carbon atoms* C*	54.04	46.35	52.49	55.48	49.75
16	*Average number of aliphatic carbon C_{al}*	30.15	24.34	30.38	33.42	27.64
17	*Average carbon number per alkyl chain*	2.76	2.90	3.43	3.96	3.02
18	*Molecular hydrogen atoms**	77.04	64.67	75.53	83.57	70.55
19	*Molecular nitrogen atoms**	0.57	0.49	0.52	0.51	0.51
20	*Molecular sulphur atoms**	2.15	1.95	2.11	2.10	2.02
21	*Molecular oxygen atoms**	6.05	1.65	0.90	0.65	3.50
22	*Average molecular weight**	899	717	795	834	795

* assuming that each molecule contains only one PAH core.

662 Table 3 ^{13}C NMR chemical shift region assignments for the asphaltene samples

Regions in ppm			**Types of Carbons**
Aliphatic	**5.0-60.0**	$\boldsymbol{C_{al}}$	
	5.0-18.0	CH_3	Terminal or branched methyl groups in aliphatic chains, except where branched at α *or* β position from an aromatic ring or where two methyl groups are terminal
	18.0-22.0	$CH_{3\ \alpha,\beta}$	Methyl groups in aliphatic chains branched at α *or* β position from an aromatic ring, plus where two methyl groups are terminal
	22.0-32.0	CH_2	Methylene groups in aliphatic chains and in naphthenic rings, except where branched at α *or* β position from an aromatic ring, or at α position from a naphthenic ring
	32.0-34.5	CH	Methine groups in aliphatic chains
	34.5-42.0	$CH_{2\ \alpha,\beta}$	Methylene groups branched at α *or* β position from an aromatic ring, or at α position from a naphthenic ring
	42.0-60.0	CH_{naph}	Methine groups in naphthenic rings
Aromatic	**100-160**	$\boldsymbol{C_{ar}}$	
	100-133	C_{br}, C_{pr}	Bridgehead aromatic carbon, overlapping with protonated/hetero aromatic carbon
	133-150	C_{sub}	Substituted aromatic carbon
	150-160	C_{phen}	Phenolic carbon

663

664

665 Table 4 AMWs estimated from MWDs using MALDI-TOF in different summation ranges and

666 from 13C NMR spectra

Summation range	AMW (Da)				
	F1	F2	F3	F4	Buton
0–1,000Da	442	474	525	558	541
0–1,500Da	714	610	709	761	743
0–2,000Da	898	755	882	957	934
0–3,000Da	1125	952	1094	1204	1177
AMW estimated from NMR/DEPT	899	717	795	834	795

667

668